



CHB STATCOM Utilization for Smoothing Power Oscillations of Fixed Speed Wind Farms

Mohammad Reza Nasiri^{a,*}

Department of Electrical Engineering, Qazvin Branch, Islamic Azad University, Qazvin, Iran

Received 07 August 2022; Accepted 13 September 2022

Abstract

Electrical output power fluctuations of wind farms inject poor quality of power into the grid. This problem is more remarkable for the wind farms utilizing fixed speed wind turbine generators (WTGs). In this paper the output power of a 10MW wind farm with 24 fixed speed WTGs, is investigated. The most appropriate location for power smoothing based on the short-term power recording and effective power oscillation frequency is determined. A transformerless cascaded H-bridge STATCOM (CHB STATCOM) combined with a mechanically switched capacitor (MSC) is proposed to compensate variable reactive power of the wind farm, as well as to smooth the short-term active power fluctuations. The active power flattening is accomplished by proper sizing of the CHB dc link capacitors according to necessary energy exchange. By comparing several distributed and centralized schemes, a 2MVar CHB STATCOM, which is economically justified, is proposed. The STATCOM performance for improving power quality of the wind farm is investigated by applying several power profiles acquired from the wind farm using simulink MATLAB environment.

key words: CHB STATCOM, wind farm, fixed speed WTG, power quality, short-term power fluctuation smoothing.

1. Introduction

Rapid growth of electricity generation from wind farms, creates more challenges for the power networks. In places where the wind power is significant among the other sources of electricity, all drawbacks of this renewable source of energy are further noticeable. Most of these problems are power quality, voltage effects (flicker, sag, swell), intermittent energy balancing using energy storage systems (ESS) and stability [1-4]. The wind turbine mechanical output power, which is proportional to the cube of wind speed, fluctuates due to many factors such as wind gusts, tower shadow effects, and wind gradient (wind shear). The fixed speed WTGs at all operating points and variable speed WTGs at less than rated power, transfer the oscillations of mechanical power to the grid [5-7].

Energy storage elements such as batteries have been proposed to smooth active power of a WTG [8, 9], and as an energy storage system for renewable energy applications [10, 11]. The supercapacitors through a

bidirectional dc/dc converter, have been used to reinforce the dc link of the WTGs including a back-to-back converter to smooth short-term fluctuations of output power [4, 12]. In a wind farm, including many turbines and high-power generation level, as the actual data show, total power fluctuations at the point of common coupling (PCC) are less than the summation of fluctuations of all turbines. Therefore, power smoothing at the PCC will impose lower energy storage capacity to the overall wind farm. On the other hand, using battery in the dc link of the STATCOM is not reasonably priced according to high generation level of the wind farm, and required cost for implementation and maintenance of the battery bank. The supercapacitors have also been used directly in the multilevel converters, like conventional capacitors, without using the bidirectional dc/dc converter for short-term active power smoothing [13, 14]. Using supercapacitors with direct integration scheme reduces the complexity and cost. However,

^a Corresponding Author. Email: mmasiri2003@ut.ac.ir

there are some drawbacks such as: 1) nonlinearity and high resistivity of supercapacitor for sudden current change, 2) voltage balancing issues for series connection of them, 3) the total energy storage capacity of the supercapacitors is not used due to their limited range of voltage variations [4, 15].

The first generation of the WTGs, which are fixed speed, generate low quality of electric power in the previously erected wind farms. These inexpensive wind farms face many challenges that are still of interest to the researchers [1, 16, 17]. This paper deals with the problem of short-term power fluctuations in the fixed speed wind farms. In this regard, short-term power generation of the fixed speed Manjil wind farm, located in the north of Iran, is investigated. Variable speed wind farms are also suffering from this problem. Many studies have been carried out to enhance power quality of an individual WTG by short-term active power smoothing. In this paper, it is shown that power quality enhancement at PCC will be more cost-effective than each one of WTGs.

The STATCOM conventionally has been used as a fast reactive power compensator, to improve power quality of the wind farms [2, 18, 19]. This paper proposes a new affordable solution to smooth short-term active power fluctuations of the fixed speed wind farm (the worst scenario), using the CHB STATCOM. The method with less cost and complexity can also be applied to the variable speed wind farms. Variable reactive power to improve voltage profile and power factor correction is assessed, and will be compensated by the same CHB STATCOM combined with the MSC, as well. The capacitance sizing of the dc links for the CHB STATCOM is presented based on the actual power profiles. It is determined by considering the period and maximum amplitude of the active power oscillation, which impacts effectively on the power quality criteria such as flicker severity. The main costs of design, i.e. the costs of dc link capacitors and high-voltage switches, in the distributed design for each WTG and centralized design at PCC, will be compared.

The designed CHB STATCOM is controlled using Model Predictive Control (MPC) algorithm with horizon one due to high dynamic performance, simplicity and intuitiveness [20-22]. Then the controlled system will be simulated with various power profiles obtained from the Manjil wind farm to evaluate the performance of the proposed system.

The paper is organized as follows; section 2 describes the undesirable effects of short-term active power fluctuations. In section 3 data recording of Manjil

wind farm and single WTG is presented. In section 4, several designs are introduced and their costs are compared, both for centralized design at PCC and distributed design for each one of WTGs. Sections 5 and 6 describe the control strategy and the simulated wind farm model, respectively. In section 7 the simulation verifications are presented. Section 8 concludes the paper.

2. Adverse Effects of the Short-Term Power Fluctuations

Short-term active and reactive power fluctuations of the wind farm produce voltage flicker [23, 24], create power oscillations in the other generators connected to the grid and degrade power quality of the overall system [25]. Active power smoothing using storage for a single generator has been reported in various studies. However, an energy storage system for the overall wind farm could be more economical by considering the location of installation and compromising between power smoothing rate and the associated cost.

2.1. Flicker Emission

Flicker emission depends on several factors such as: mean wind speed, turbulence intensity, wind speed gradient (wind shear), tower shadow effect, short-circuit capacity ratio and grid impedance angle. Tower shadow effect and wind speed gradient lead to power fluctuation in the frequency equal to triple of blade's rotational speed. This frequency is referred to as $3p$ frequency. Output power of the WTGs (fixed speed, variable speed at less than rated power, and even variable speed with full-scale back-to-back converter) fluctuates with this frequency [5, 6, 23].

The flicker is mainly emanated by fluctuations of active power produced by a wind farm [5, 23, 26]. Unlike the conventional method, where flicker mitigation is performed by controlling the reactive power proportional to active power [6], active power smoothing is more effective, especially in the weak networks where the grid impedance angle is low.

According to IEC 61000-4-15 standard, flicker severity is measured by short-term flicker severity p_{st} , a measurement associated with noticeable flicker of incandescent lamps and human perception system. Fig. 1 shows the flicker severity p_{st} versus the frequency of power variations. This curve has been sketched for a relative rectangular voltage change of 2.4%. As it can be seen p_{st} between 1Hz up to 8.8Hz, increases with high slope. Unfortunately, the $3p$

frequency of the fixed speed wind turbines usually falls within this range. The 3p frequency fluctuation of active power is the most significant part in the flicker emission [23]. Using energy storage elements for active power smoothing at less than 1Hz needs high energy storage capacity at the high generation level.

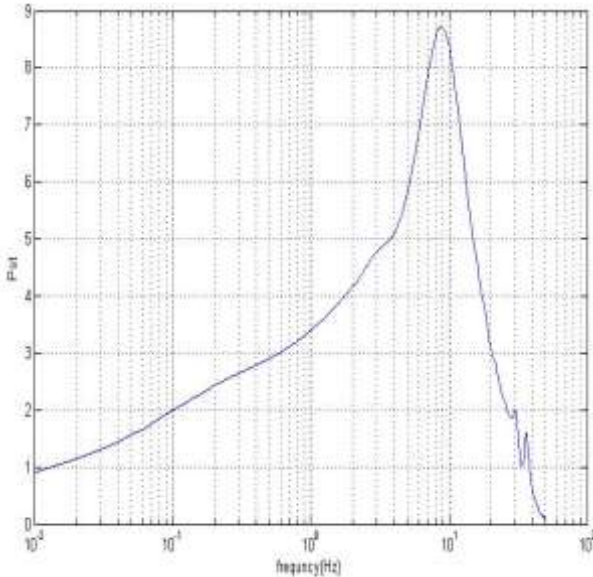


Fig. 1. p_{st} versus frequency for 2.4% rectangular voltage fluctuation

2.2. Stimulating Natural Frequencies of the Power System

Wind power fluctuations act as an external disturbance to the power system. The 3p frequency of the power fluctuations generated by the wind farm in the continuous operation, tends to coincide with the inter-area oscillations of the power system. Therefore, these 3p power oscillations act like a source, that can stimulate resonant oscillation frequencies of the power system. Reference [25] has studied the effect of 3p power oscillations of a wind farm with fixed speed WTGs on the Irish power system by analyzing the actual data. The authors in [27] have shown by simulation, that the 3p frequency oscillations of wind power, may stimulate the power system with a frequency close to the natural oscillation frequencies.

Therefore, according to above discussions, smoothing of the short-term power fluctuation (3p frequency) will be considered in the next sections.

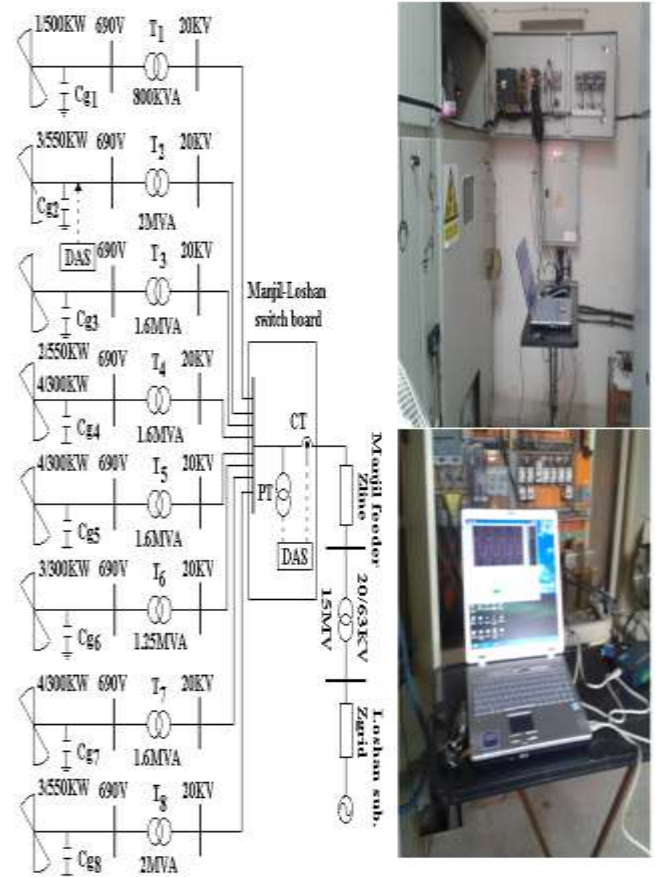


Fig. 2. Data monitoring at Manjil wind farm, (a) wind farm single line diagram and data recording locations, (b) data recording at Manjil-Loshan switch board (up) and the unit 2 of Manjil wind farm (bottom).

3. Manjil Wind Farm

Manjil windy area is located at the north of Iran. There are five separate wind farms (sites) in this area, which are connected to the national grid in three points through eight different feeders. These sites are Manjil, Pascolan, Rudbar, Harzevil and Siahposh. The Manjil wind farm, which is investigated in this paper, contains 24 fixed speed stall controlled WTGs with rated powers of 500kW (one unit), 550 kW (eight units), and 300 kW (15 units). This wind farm is connected to Loshan substation through the switch board Manjil-Loshan and feeder Manjil.

Fig. 2 (a) illustrates the single-line diagram of the wind farm.

The Manjil area has continuous and high speed wind between March up to September. The wind farm performance data has been recorded in late August, both at Manjil-Loshan switch board and at unit 2 of Manjil with sample rate 8kS/sec. These locations are also denoted in

Fig. 2 (a).

Fig. 2 (b) shows the data acquisition equipments during recording of data.

3.1.Power Profile of a Single WTG

Unit 2 of Manjil wind farm is a 550 kW stall controlled fixed speed WTG. Fig. 3 (a) shows the phase voltage and current waveforms which are sampled simultaneously for calculation of power profiles. Fig. 3 (b) shows 12-second profiles of the WGT output active and reactive powers. The rotor speed meter of the wind turbine was showing the average speed of 27 rpm during the data acquisition. Therefore, the 3p frequency is $3 \times 27 / 60 = 1.35$ Hz. In Fig. 3 (b), the average value of the output active power varies about 30% peak to peak with this frequency. The output power of the WTG also oscillates at the frequency of 100 Hz, that is due to the three-phase currents, including the negative sequences. The reactive power also oscillates both with 3p frequency and 100 Hz. Reactive power average value is about 50% of the average active power.

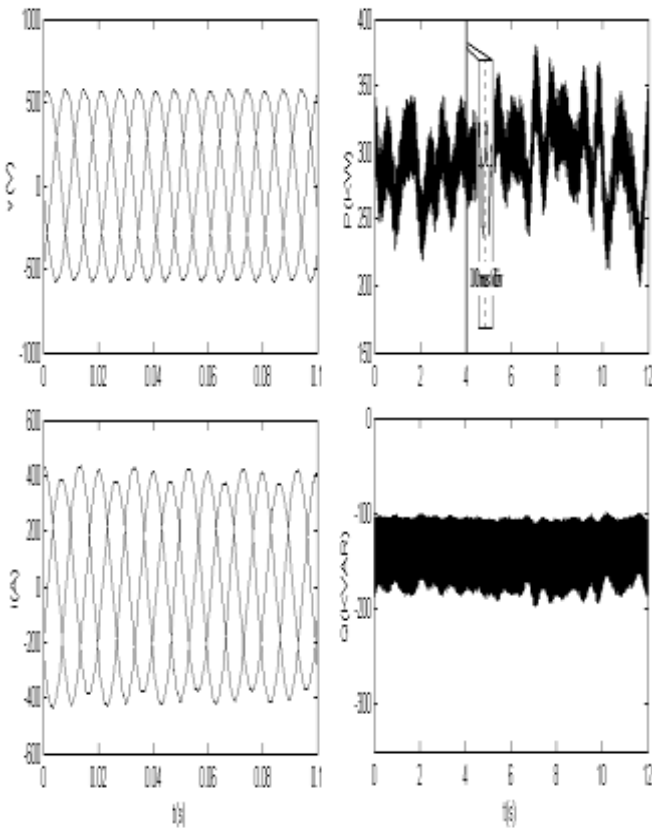


Fig. 3. Unit 2 of Manjil wind farm profiles, (a) Three phase voltage and current waveforms, (b) Active and reactive powers.

3.2.Total Power Profile

The Manjil wind farm can inject total power of 10.34 MW into the grid. Fig. 4 shows 12-second output active and reactive power profiles of the wind farm at the instant of measurement. The 3p frequency oscillations can be seen clearly in the active power, but the average power varies about 14% peak to peak with this frequency. The percentage of power variations is almost half of the oscillations' amplitude of a single WTG. Therefore, power smoothing at the PCC needs smaller storage capacity compared to the total capacity required for each WTG in the overall wind farm. The wind farm reactive power also oscillates with the 3p frequency but with smaller amplitude.

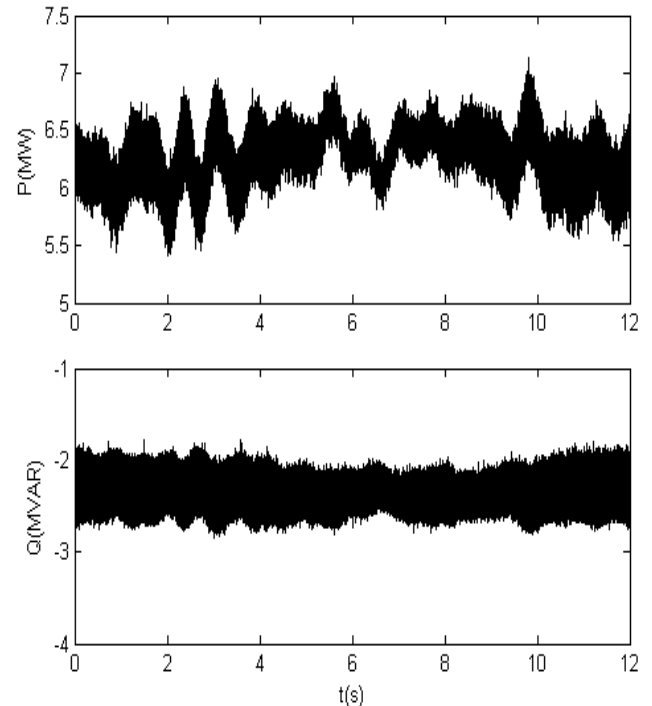


Fig. 4. Manjil wind farm output active and reactive powers.

4.Design Concept of the CHB STATCOM

Design presented here is relied on the data of Manjil wind farm. However, it is possible to apply to other wind farms by using appropriate design parameters and quantities. Fig. 5 shows a 10.34 MW wind farm connected to a 200 MVA, 63kV network through a 12 km feeder, and a 20/63 kV, 15 MVA transformer. The system specifications are given in table 1. According to recorded data, the maximum reactive power that the wind farm absorbs from the grid is equal to 5 MVar at the rated power generation. The injected active power to the grid fluctuates with the maximum values of ± 0.75 MW ($\pm 7.5\%$) at the PCC. The

frequency of fluctuations is nearly 1.3 Hz, which is almost constant for the wind farm, including fixed speed WTGs. However, the active power also fluctuates with other frequencies less than 1.3 Hz due to several factors discussed in section 2. Design based on these lower frequencies leads to higher storage sizing and cost. Fortunately, these low-frequency fluctuations have fewer effects on the power quality criteria such as flicker severity [23]. In the following, some limiting factors are discussed, affecting integration of the wind farm to the network.

4.1.Limiting Factors for Grid Integration of the Wind Farm

In addition to disadvantages detailed in section 2, there are some other limitation factors for wind farm connection to a weak or distribution grid, including:

- 1) Overvoltage is an important factor, which should be less than permissible limit 5%. In Fig. 5, without considering STATCOM and MSCs, a close approximation for voltage drop (rise) at the PCC is given by

$$\Delta V_s \cong R_{line} P_w + X_{line} Q_w \tag{1}$$

where R_{line} and X_{line} are the resistance and inductance of the line impedance, P_w and Q_w are output active and reactive power of the wind farm, respectively. All values are in per unit. Improvement of voltage profile using var compensation for a weak grid with low X/R, under the high generation level, needs high amount of reactive power, leading to more power loss in the involved grid components such as transformers and transmission lines.

- 2) Overloading of the involved grid components, which depends on the thermal rating of them.
- 3) Harmonic emission of the WTGs including power electronic converters, in the variable speed wind farms.

Using **Error! Reference source not found.** maximum overvoltage at the PCC for unity power factor operation of the wind farm is computed equal to 3.3% and 4.7% , when the on-load tap changer (OLTC) of the transformer 20/63 kV is in active and inactive states, respectively. These values are in the permissible range in both situations; therefore, unity power factor operation is selected for the wind farm to reduce power losses and to avoid overloading of the

involved components.

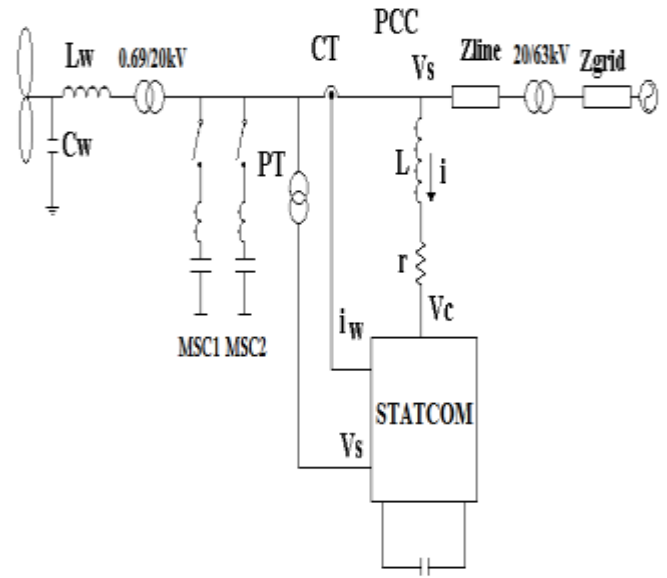


Fig. 5. Single line diagram of the grid connected wind farm equipped with STATCOM and MSC.

Table 1
Grid connected wind farm parameters

	power	volt. (kV)	resist.* (Ω)	react.* (Ω)	freq. (Hz)
wind farm	10.34 MW	20	-	-	50
12Km feeder	-	20	1.3136	3.9582	50
grid+trans.	200 MVA	20	0.5373	3.2865	

* All parameters have been transferred to 20kV side.

4.2.Centralized Design at PCC

Variable and fluctuating reactive power of the wind farm needs a dynamic var compensator. By combining two types of steady state and dynamic schemes, a cost effective dynamic var compensator can be achieved. The combination of 3 MVar MSC (with two 1.5 MVar steps), and 2 MVar STATCOM ($\approx 20\%$ of the wind farm generation capacity) is proposed for dynamic var compensation, as well as short-term active power smoothing of the wind farm. The MSC is almost lossless, benefits low-cost and

complexity. However, larger capacity of MSC (with more steps) together with smaller capacity of STATCOM deteriorates the power quality of the wind farm by frequent switching of the MSC due to variable wind speed.

A simplified single-line diagram of the main circuit, including STATCOM and MSC is shown in Fig. 5. The current rating of the STATCOM can be determined using,

$$\sqrt{\Delta P^2 + Q^2} = \sqrt{3}V_s I \quad (2)$$

where ΔP , Q and V_s are the active power variations, reactive power and line voltage, respectively. After substituting the related values into **Error! Reference source not found.**, the current rating of the STATCOM will be equal to 61.6A.

Minimum dc bus voltage per phase for reactive power compensation can be found by:

$$V_{dc_Pmin} = \sqrt{2}|Z|\left(\frac{Q}{\sqrt{3}V_s}\right) + \sqrt{2}\left(\frac{V_s}{\sqrt{3}}\right) \quad (3)$$

where $|Z|$ is the magnitude of smoothing impedance, that is considered equal to 9.3Ω (5% in per unit). Substituting the relevant values into **Error! Reference source not found.**, results in $V_{dc_pmin} = 17.09$ kV. The maximum value of the dc bus voltage depends on the voltage rating of power electronic switches, and the number of HB cells per phase.

The capacitance sizing for each dc link, with the aim to smooth the active power depends on the: 1) frequency of fluctuations, 2) amplitude of compensating power change, 3) waveform of the short-term active power variations, and 4) allowed range of dc link voltage variations. The design is carried out with frequency of 1.3 Hz, which is nearly equal to the 3p frequency of each turbine in the wind farm. The waveform is considered rectangular for the worst case. The allowed range of the dc link voltage variation is determined from the max and min values of the dc bus voltage, and the number of cells in each phase. The required capacitance of each dc link can be calculated according to (4):

$$\begin{aligned} \Delta E &= (2\Delta P)\frac{T}{2} = \frac{1}{2}nC\left((V_{dc0} + \Delta V)^2 - (V_{dc0} - \Delta V)^2\right) \quad (4) \\ &= 2nC V_{dc0} \Delta V \end{aligned}$$

where ΔE and ΔV are the total energy exchange and allowed voltage change for each dc link, respectively. n is the total number of dc links. T is the variations period equals to 1/1.3 s, and V_{dc0} is the dc link operating point voltage. Replacing corresponding values into (4), the capacitance of each dc link is determined. Table 2 summarizes several centralized designs using 3.3 kV, 4.5 kV and 6.5 kV IGBTs for a single CHB STATCOM at the PCC.

Table 2
Several centralized designs of the CHB STATCOM at the PCC

dual IGBT (kV,A,\$)	cells p. ph.	dc link* max volt. (kV)	V_{dc0} (kV)	ΔV (V)	C (mF)	total price (cap.+sw.) (US \$)
3.3,100, 549.7	10	2(60%)	1.85	± 145	35.6	93090
"	11	"	1.77	± 223	22	76932
4.5,150, 626.8	7	3(60%)	2.72	± 279	18.07	74834
"	8	"	2.56	± 432	10.8	63322
6.5,85, 689	6	4(60%)	3.42	± 576	8.1	58040
"	7	"	3.22	± 779	5.5	55180
"	8	"	3.07	± 932	4.2	55962

* dc link max voltage has been considered equal to 60% of the switch voltage.

Table 3
Several designs for 550kW and 300kW WTG units, smoothing react. 20%, active power fluctuations $\pm 15\%$.

unit	dual IGBT (kV,A,\$)	cells no. p. phase	V_{dc0} (kV)	ΔV (V)	C (mF)	total price (cap.+sw.) (US \$)
550kw	1.2,200,156	1	0.687	± 33	510.1	12202
	"	2	0.523	± 196	56.5	4369
	"	3	0.468	± 251	33.3	4990
300kw	1.2,100,97.2	1	0.686	± 33	277	6694
	"	2	0.523	± 196	30.8	2528
	"	3	0.468	± 251	18	2939

Minimum total cost for (9/550kw+15/300kw) units = 77241\$

4.3. Distributed Design and Cost Comparison

In table 3 similar designs have also been carried out for the 550 kW and 300 kW WTGs by considering 10% overgeneration, and 121 kVar, 66 kVar, reactive power, respectively.

High-voltage switches such as IGBTs are expensive. So, they can also significantly impact on the total price of the CHB STATCOM with energy storage ability. To demonstrate which design provides the lowest cost, in addition to the storage costs, switches' costs must also be considered. The switches in tables 2 and 3 are selected from Powerex products. In these tables the total price (capacitors + switches) are calculated using electrolytic capacitor cost about 28.4\$/kJ in the market for the max voltage of dc link, and dual IGBT price from Powerex.

In table 2, the configuration of seven cells per phase using 6.5 kV, 85A IGBT leads to minimum cost and reasonable number of cells, for the centralized design at PCC.

Table 3 shows minimum cost design is the two HB cells in each phase for both 550 kW and 300kW units. From this table, the minimum total cost of the distributed design for the 24 units of the wind farm, is 40% higher than the minimum cost of the centralized design at the PCC. Furthermore, other expenses such as costs of control system, casing, maintenance, etc. for the 24 units will also be higher than the similar costs for the single design at the PCC. Therefore, the comparisons confirm the design at PCC, is more cost effective. Accordingly, seven cells per phase CHB STATCOM at PCC is selected. Schematic diagram of the transformerless seven cells CHB STATCOM is shown in

Fig. 6. Table 4 also summarizes the design parameters.

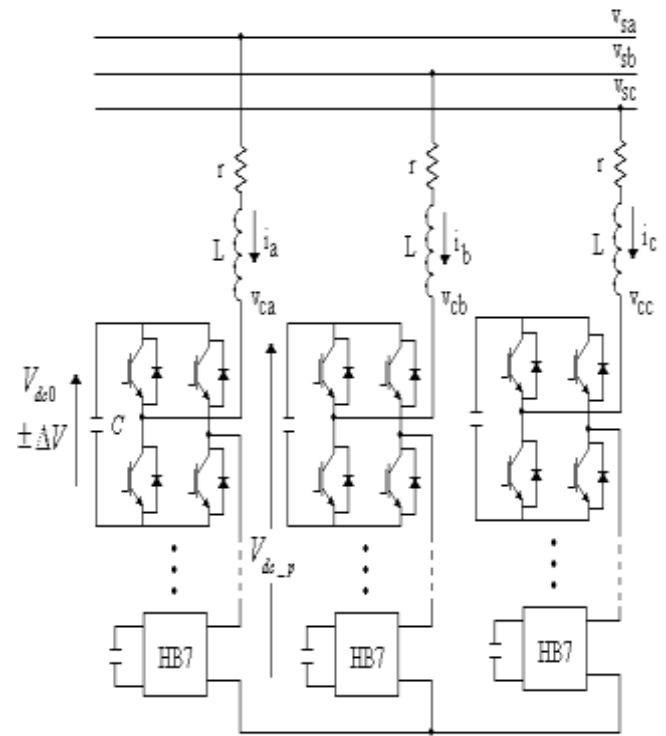


Fig. 6. Transformerless seven cells CHB STATCOM

Table 4
Parameters of the CHB STATCOM design

parameter	value	parameter	value
voltage	20 kV	ΔE	0.57 MJ
current	61.6 A	react. (5%)	9.3 Ω
Q	2 MVar	$V_{dc0} \pm \Delta V$	3.22 ± 0.778 kV
ΔP	± 0.75 MW	C	5.5 mF

Switch type: 6.5 kV, 85 A dual IGBT, QID6508001, Powerex

5. Control Strategy

Fig. 7 (a) shows the control system of the CHB STATCOM in Fig. 5 and

Fig. 6. The command signals for active power variations are applied from two points into the control system, creating more efficient control in terms of abrupt and slow fluctuations of the active power.

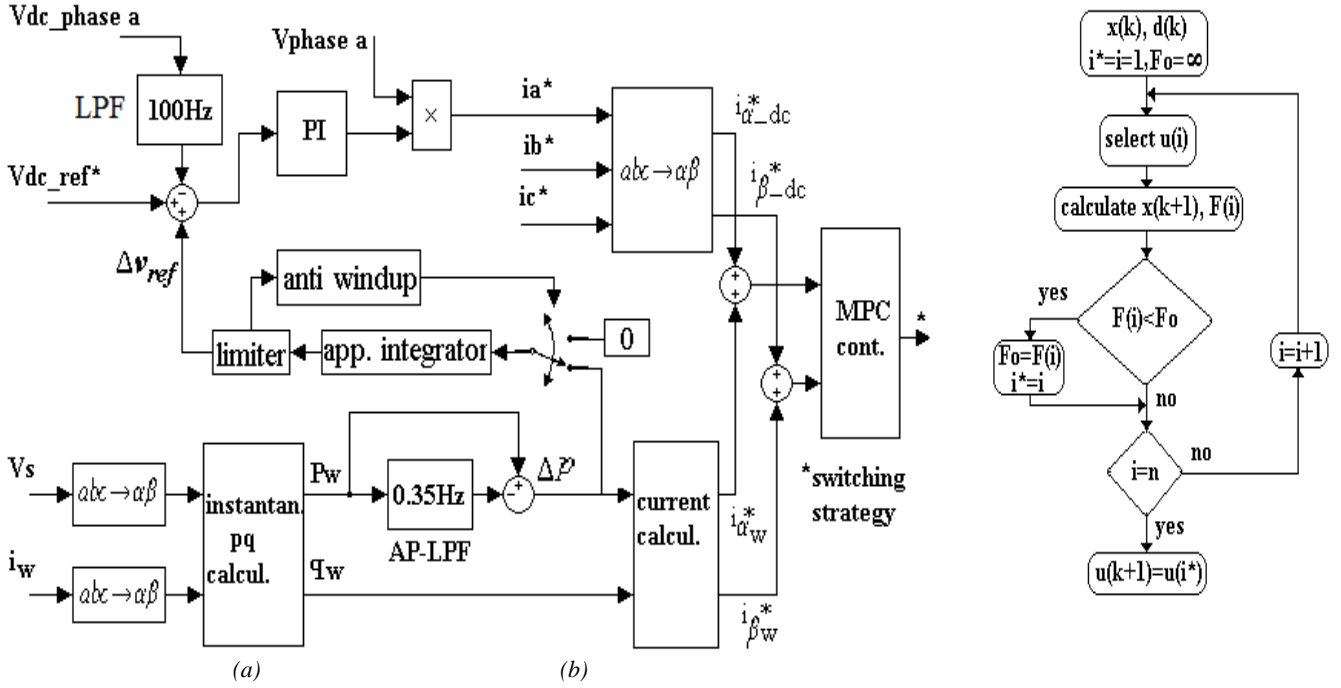


Fig. 7. (a) CHB STATCOM control block diagram, (b) Predictive control algorithm.

5.1. Command Signal

In the block diagram shown in Fig. 7 (a), the active and reactive powers of the wind farm are calculated based on the instantaneous power theory [28]. The active power is filtered by a second-order lowpass filter (AP-LPF) to extract the variable component by subtracting the input from the output. The resultant filter cutoff frequency f_{CH} in terms of AP-LPF cutoff frequency f_{CL} , according to the slope of the tangent to the curve of bode diagram of the resultant filter is obtained as,

$$\frac{20 \log \frac{1}{\sqrt{2}} - 20 \log \left(1 - \frac{1}{\sqrt{2}} \right)}{\log(2\pi f_{CH}) - \log(2\pi f_{CL})} \cong 20 \text{ db/dec}, \quad (5)$$

resulted in,

$$f_{CH} \cong (1 + \sqrt{2}) f_{CL}. \quad (6)$$

To filter out the active power fluctuations, f_{CH} needs to be selected less than power fluctuation frequency 1.3 Hz, or f_{CL} less than 0.54 Hz. Therefore, pass band of AP-LPF (f_{CL}) is selected to be 0.35Hz. The current reference signals, in the stationary coordinate system $\alpha - \beta$ are calculated from the reactive power and variable component of the active power. They are used as command signals to the MPC. The reactive power of the wind farm can be compensated completely for the unity power factor operation. However, active power smoothing needs another command to charge and discharge of the dc link capacitors.

Reference signal for the dc bus voltage includes a constant value added to a variable value, which is provided by the variable component of active power. The dc bus voltage variation reference is derived by considering the variations of stored energy of each capacitor,

$$\Delta e \approx CV_{dc0} \Delta v_{dc} \quad (7)$$

where Δe is the energy exchange and Δv_{dc} is each dc link voltage variations. The variable value of the reference signal for total dc bus voltage will be,

$$\Delta v_{ref} = \frac{n}{3} \Delta v_{dc} \approx \frac{n}{3CV_{dc0}} \Delta e = \frac{n}{3CV_{dc0}} \times \frac{1}{n} \int \Delta p dt \quad (8)$$

where Δp is the variable component of active power. Substituting corresponding values into **Error! Reference source not found.**, the integral gain is obtained as $K_I = 18.82 \times 10^{-3}$ V/J. Open loop integration is unstable practically, so an appropriate stable lowpass filter is used as,

$$\frac{K_p}{1 + \tau_n s} \quad (9)$$

To make this lowpass filter act as an integrator, cutoff frequency $1/2\pi\tau_n$, should be very smaller than Δp variations' frequency. The integral gain is computed using $K_I = K_p/\tau_n$. Therefore, $\tau_n = 1.65$ s is selected and K_p is obtained equal to 0.031 VS/J for the variations' frequency of 1.3 Hz. This block has been denoted by app. integrator in Fig. 7 (a). A limiter is used for limiting of the dc link voltage variations in predefined range. When the output of app. integrator reaches to the upper or lower band, the input is changed to zero until the sign of Δp changes (anti windup limiter).

5.2. Model Predictive Control

MPC algorithm in each sample time k , begins by measuring state variables $x(k)$ and disturbances $d(k)$. Using these measured values and discrete model of the system, the next state variables $x(k+1)$ are predicted for each possible input u . A cost function F over the state variables $x(k+1)$ and reference values $x^*(k+1)$ is optimized in a loop. The input u^* minimizing the cost function is applied to the system at beginning of next sample time [22, 29], i.e.

$$u(k+1) = u^* \quad (10)$$

The algorithm is depicted in Fig. 7 (b). The optimization loop could be eliminated by direct solution of the cost function [29]. This algorithm

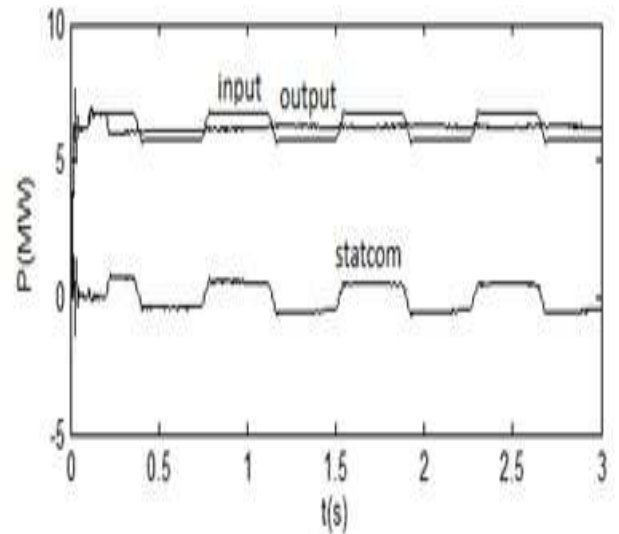
benefits high dynamic performance and low complexity. This control method is applied to the STATCOM as a current controlled voltage source inverter. The detailed discussion of the control method is out of the paper's scope.

6. Wind Farm Simulated Model

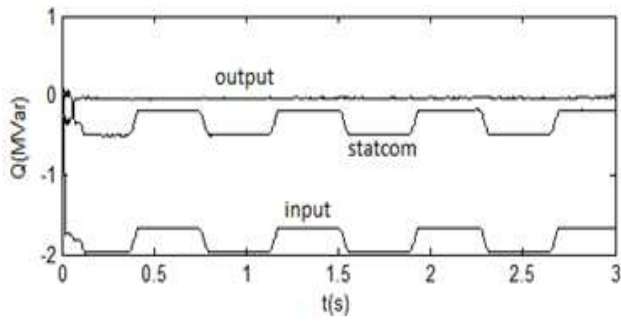
The focus of this paper is on the electric power flow of the wind farm during continuous operation by applying actual data (power profiles). Therefore, the model of the wind farm does not include mechanical and electrical dynamic model of each WTG in the wind farm [3]. The real three phase sampled currents of Manjil wind farm are fed into the grid using controlled current sources in the simulink environment. Applying real data of the wind farm take advantage of considering each WTG in its real specific conditions among the others, which is important in this study. The phase of the voltage source for the Thevenin equivalent of the grid is lagged by $\tan^{-1}(-Q/P)$ with respect to the sampled currents.

7. Simulation Results

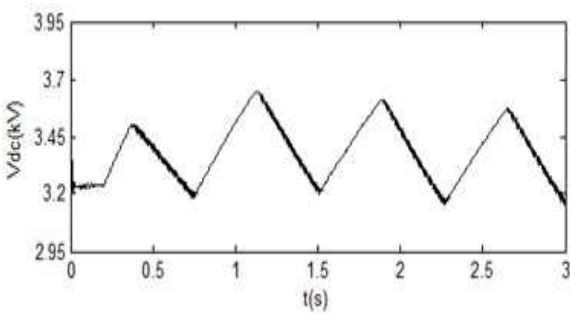
The simulations have been carried out using simulink toolbox of MATLAB software. Operation of the system is demonstrated by applying different active power fluctuations and reactive power step changes. The system performance is investigated under the wind gust power profile. The effects of parameter variation of the MPC controlled STATCOM is also studied.



(a)



(b)



(c)

Fig. 8. 6MW active power modulated by a square wave of frequency 1.3 HZ and amplitude 0.5MW, (a) Input, output to the grid, and STATCOM active powers, (b) Input, output, and STATCOM reactive powers, (c) The dc link voltage variations.

7.1. Square Wave Power Variations and MPC

Dynamics

The STATCOM has been designed to smooth square wave power oscillations and also to compensate the reactive power. The active power is set to about 6 MW modulated by a 1.3 Hz square wave and about 0.5MW amplitude. The STATCOM starts to compensate reactive power at 0.05 s. The power variation is initiated at 0.1 s, and smoothing of active power begins at 0.2s.

The smoothed active power is supplied to the grid, and its fluctuation is absorbed by the STATCOM as shown in Fig. 8 (a). Fig. 8 (b) shows the reactive power, and its variations are completely compensated by the CHB STATCOM and one of 1.5 MVar MSC. In Fig. 8 (c) charging and discharging of the dc link is shown around the set value 3.22 kV. Dynamic performance of the MPC is demonstrated by applying a reactive power command change

between zero and rated value, whereas the command for variable component of active power is kept zero. Therefore, the command signal is just directly applied to the MPC, and the dc bus command signal will remain constant. The dynamic response of the corresponding current in one phase is shown in **Error! Reference source not found.** The output current tracks the input command after 2 ms.

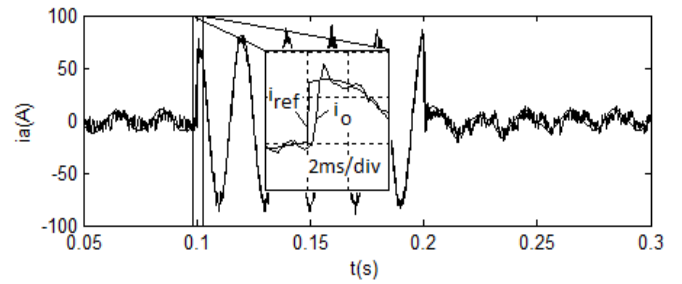
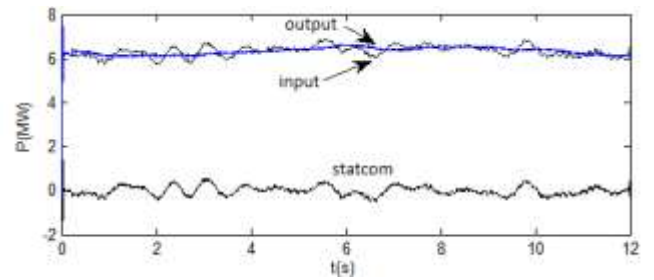
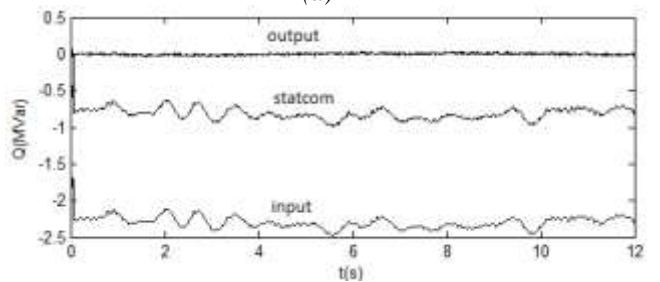


Fig. 9. MPC dynamic performance for reactive power step change of 100%. Reference and output currents of phase a.



(a)



(b)

Fig. 10. Normal operation, (a) Input, output to the grid, and CHB STATCOM average active powers, (b) Input, output, and CHB STATCOM average reactive powers.

7.2. Normal Operation

The 12-second power profile generated by Manjil wind farm, which was investigated in section 3 (Fig. 4), is fed to the grid. Fig. 10 shows active and reactive average powers within the system, i.e. wind farm

generation, CHB STATCOM absorption, and injected power into the grid. Reactive power is completely compensated. The short-term fluctuation of the injected power is also eliminated, so that the output active power tracks the mean value of the input power coming from the wind farm.

7.3.Operation Under the Wind Gust

Fig. 11 (a) depicts the output active power generated by the wind farm, where the wind speed suddenly initiates to change at 2s. The active power is reduced about 30%. The output average power to the grid and the CHB STATCOM absorption, as well as the output average reactive powers are shown in Fig. 11 (b). Between about 3s up to 4.5s active power smoothing ability of the CHB STATCOM has been stopped, due to suddenly the reduction of the input power, and consequently, saturation of the dc links voltage on the allowed boundary value. Outside of this time interval, output active power tracks fairly the input mean value. Reactive power is compensated at all times.

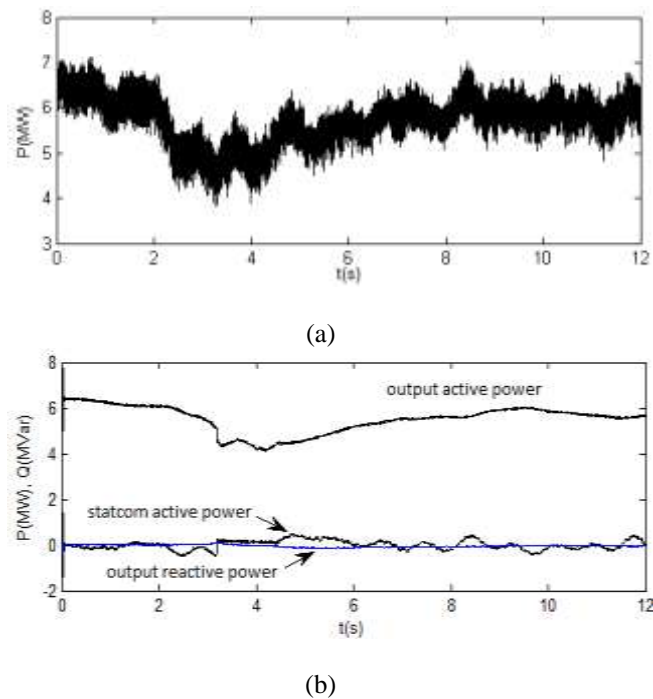


Fig. 11. Operation under the wind gust, (a) Generated active power of the wind farm. Wind speed reduction has been occurred at 2s, (b) Output to the grid and the CHB STATCOM absorption average active powers, as well as output average reactive power.

7.4.Dependency on Parameter Variations

The quality of the injected power into the grid depends on the operation of the CHB STATCOM and its parameters.

The pass band of the AP-LPF, is an important parameter which impacts on the short-term power smoothing. Fewer cutoff frequency yields better result, however, the voltage of dc links may reach to their allowed limit values. To investigate this effect, cutoff frequency of the low-pass filter is increased and decreased to 0.55 Hz and 0.15 Hz. **Error! Reference source not found.** shows the effects of increasing and decreasing of the pass band on the average output power and the dc link voltage. As it can be seen 0.35 Hz is the well tuned pass band for the AP-LPF.

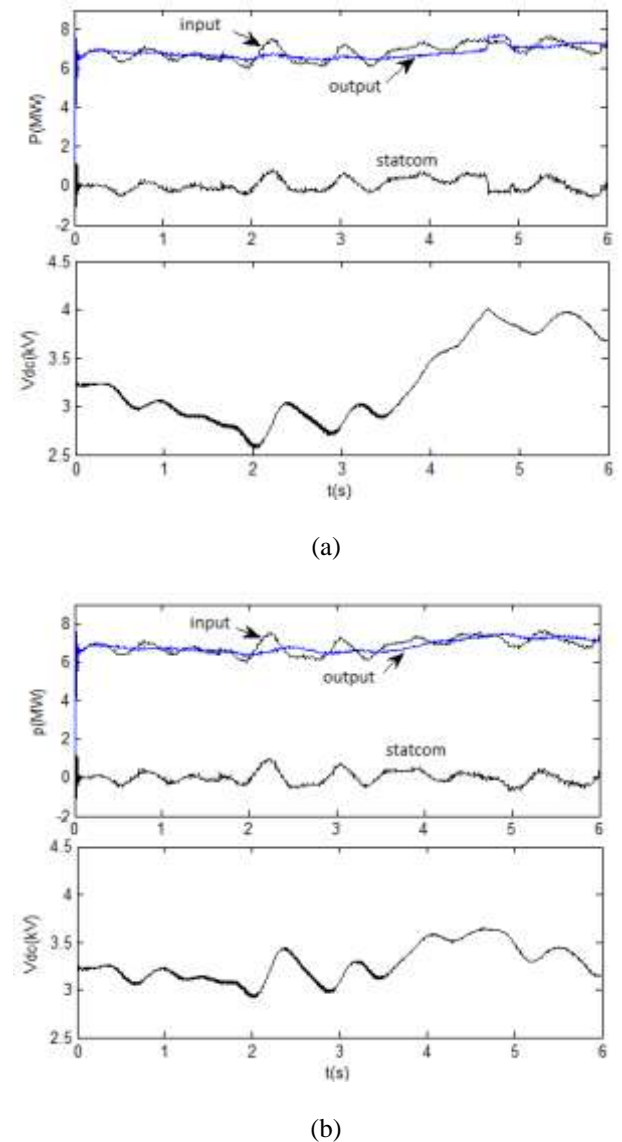


Fig. 12. AP-LPF pass band variation effects, (a) Average active powers and dc link voltage at pass band 0.15Hz, (b) Average active powers and dc link voltage at pass band 0.55Hz.

8. Conclusion

This paper dealt with the problem of short-term power fluctuations in the wind farms with fixed speed WTGs. In this regard, Manjil wind farm, including 24 fixed speed WTGs was studied. Short-term active and reactive power profiles of the wind farm and one of the production units, were obtained by simultaneous sampling of current and voltage waveforms. Investigation on the real data revealed that the short-term active power smoothing to improve power quality indices, at the PCC will be more cost-effective than each of the individual WTGs in a wind farm.

This study, based on empirical data, proposed the CHB STATCOM, without using battery bank or supercapacitors, to remove short-term oscillatory components of the wind farm power generation. Accordingly, a transformerless CHB STATCOM combined with MSC was used to compensate variable reactive power, as well as to smooth short-term fluctuations of active power produced by the wind farm. Capacitance sizing of the dc links was modified to appropriate energy exchange. The main costs of design, i.e. costs of the dc link capacitors and high-voltage switches, for the distributed design and centralized design were compared to confirm that the centralized design imposes minimum cost to the whole wind farm. Although the design was relied on the data of Manjil wind farm, but the proposed design procedure can be easily applied to other wind farms by optimizing the capacitance sizing of dc links and number of CHB cells.

Simulations were presented based on various power profiles acquired from Manjil wind farm. Several conditions such as wind gust and parameter dependency of the CHB STATCOM were investigated using real data. The simulation results demonstrated that the combination of CHB STATCOM with MSC at PCC provide a cost-effective solution for reactive power compensation, fast response time, and short-term active power smoothing of the wind farm to enhance the power quality.

References

- [1] M. Rahimi and H. Assari, "Addressing and assessing the issues related to connection of the wind turbine generators to the distribution grid," *International Journal of Elect. Power & Energy Syst.*, vol. 86, pp. 138-153, 2020.
- [2] Y. K. Gounder, N. Devarajan, and V. Boominathan, "Enhancement of transient stability of distribution system with SCIG and DFIG based wind farms using STATCOM," *IET Renewable Power Gen.*, vol. 10, no. 8, pp. 1171 - 1180, 2018.
- [3] C. Han, A. Q. Huang, M. E. Baran, S. Bhattacharya, W. Litzemberger, L. Anderson, A. L. Johnson, and A. Edris, "STATCOM impact study on the integration of a large wind farm into a weak loop power system," *IEEE Trans., Energy conv.*, vol. 23, no. 1, pp. 226-233, 2008.
- [4] C. Abbey and G. Joos, "Supercapacitor energy storage for wind energy applications," *IEEE Trans., Industry App.*, vol. 43, no. 3, p. 769, 2010.
- [5] A. Larsson, "Flicker emission of wind turbines during continuous operation," *IEEE Trans., Energy Conv.*, vol. 17, no. 1, pp. 114-118, 2002.
- [6] T. Sun, Z. Chen, and F. Blaabjerg, "Flicker study on variable speed wind turbines with doubly fed induction generators," *IEEE Trans., Energy conv.*, vol. 20, no. 4, pp. 896-905, 2005.
- [7] M. Liserre, R. Cardenas, M. Molinas, and J. Rodriguez, "Overview of multi-MW wind turbines and wind parks," *IEEE Trans., Indust. Elec.*, vol. 58, no. 4, pp. 1081-1095, 2011.
- [8] X. Li, "Fuzzy adaptive Kalman filter for wind power output smoothing with battery energy storage system," *IET Renewable Power Gen.*, vol. 6, no. 5, pp. 340-347, 2021.
- [9] S. W. Mohod and M. V. Aware, "A STATCOM-control scheme for grid connected wind energy system for power quality improvement," *IEEE, Systems Journal*, vol. 4, no. 3, pp. 346-352, 2010.
- [10] S. Ahmad Hamidi, D. M. Ionel, and A. Nasiri, "Modeling and Management of Batteries and Ultracapacitors for Renewable Energy Support in Electric Power Systems—An Overview," *Electric Power Components and Systems*, vol. 43, no. 12, pp. 1434-1452, 2015.
- [11] S. Teleke, M. E. Baran, S. Bhattacharya, and A. Q. Huang, "Optimal control of battery energy storage for wind farm dispatching," *IEEE Trans., Energy conv.*, vol. 25, no. 3, pp. 787-794, 2020.
- [12] G. Xu, L. Xu, and D. Morrow, "Wind turbines with energy storage for power smoothing and FRT enhancement," in *Power and Energy Society General Meeting, IEEE*, pp. 1-7, 2011.

- [13] S. G. Jayasinghe and D. M. Vilathgamuwa, "Flying Supercapacitors as Power Smoothing Elements in Wind Generation," *IEEE Trans., Indust. Elec.*, vol. 60, no. 7, pp. 2909-2918, 2013.
- [14] L. Maharjan, S. Inoue, and H. Akagi, "A transformerless energy storage system based on a cascade multilevel PWM converter with star configuration," *IEEE Trans., Industry App.*, vol. 44, no. 5, pp. 1621-1630, 2008.
- [15] H. El Fadil, F. Giri, J. M. Guerrero, and A. Tahri, "Modeling and nonlinear control of a fuel cell/supercapacitor hybrid energy storage system for electric vehicles," *IEEE Trans., Vehicular Tech.*, vol. 63, no. 7, pp. 3011-3018, 2019.
- [16] M. Wei and Z. Chen, "Fast control strategy for stabilising fixed-speed induction-generator-based wind turbines in an islanded distributed system," *IET Renewable Power Gen.*, vol. 7, no. 2, pp. 144-162, 2013.
- [17] S. Sharma and B. Singh, "Performance Evaluation of Fixed-speed and Variable-speed Stand-alone Wind Energy Conversion Systems," *Electric Power Components and Systems*, vol. 44, no. 4, pp. 402-410, 2016.
- [18] A. Manori, M. Tripathy, and H. O. Gupta, "Advance compensated Mho relay algorithm for a transmission system with shunt flexible AC transmission system device," *Electric Power Components and Systems*, vol. 42, no. 16, pp. 1802-1810, 2014.
- [19] B. Singh, S. Murthy, and R. S. R. Chilipi, "STATCOM-based controller for a three-phase seig feeding single-phase loads," *IEEE Trans., Energy conv.*, vol. 29, no. 2, pp. 320-331, 2014.
- [20] M. Abdelrahem and R. Kennel, "Efficient Direct Model Predictive Control for Doubly-Fed Induction Generators," *Electric Power Components and Systems*, vol. 45, no. 5, pp. 574-587, 2017.
- [21] T. Shi, C. Zhang, Q. Geng, and C. Xia, "Improved model predictive control of three-level voltage source converter," *Electric Power Components and Systems*, vol. 42, no. 10, pp. 1029-1038, 2014.
- [22] J. Rodríguez, J. Pontt, C. A. Silva, P. Correa, P. Lezana, P. Cortés, and U. Ammann, "Predictive current control of a voltage source inverter," *IEEE Trans., Indust. Elec.*, vol. 54, no. 1, pp. 495-503, 2007.
- [23] W. Hu, Z. Chen, Y. Wang, and Z. Wang, "Flicker mitigation by active power control of variable-speed wind turbines with full-scale back-to-back power converters," *IEEE Trans., Energy conv.*, vol. 24, no. 3, pp. 640-649, 2009.
- [24] G. Joos, "A short-term energy storage system for voltage quality improvement in distributed wind power," *IEEE Trans., Energy conv.*, vol. 29, no. 4, pp. 997-1007, 2014.
- [25] S. Brownlees, D. Flynn, B. Fox, and T. Littler, "The impact of wind farm power oscillations on the Irish power system," in *Power Tech., 2007 IEEE Lausanne*, pp. 195-200, 2007.
- [26] T. L. Van, T. H. Nguyen, and D.-C. Lee, "Flicker suppression scheme for variable-speed wind turbine systems," *Journal of Power Elect.*, vol. 12, no. 2, pp. 333-343, 2012.
- [27] W. Hu, C. Su, and Z. Chen, "Impact of wind shear and tower shadow effects on power system with large scale wind power penetration," in *IECON Annual Conf. IEEE Industrial Elect.*, pp. 878-883, 2011.
- [28] H. Akagi, E. H. Watanabe, and M. Aredes, *Instantaneous power theory and applications to power conditioning* vol. 31: John Wiley & Sons, 2007.
- [29] [M. A. Pérez, P. Cortés, and J. Rodríguez, "Predictive control algorithm technique for multilevel asymmetric cascaded H-bridge inverters," *IEEE Trans., Indust. Elec.*, vol. 55, no. 12, pp. 4354-4361, 2008.